AD-A067 557 NAVAL POSTGRADUATE SCHOOL MONTEREY CALIF F/G 4/1
AN EXPERIMENTAL SYSTEM TO MEASURE ATMOSPHERIC EXTINCTION OF VIS--ETC(U)
DEC 78 J R MACDONALD

UNCLASSIFIED NL

| OF |
AD
A067557

END
DATE
FILMED
6-79
DDC

NAVAL POSTGRADUATE SCHOOL
Monterey, California

THESIS

An Experimental System To Measure Atmospheric Extinction Of Visible, Near and Far Infrared Radiation In The Marine Boundary Layer

by

J.R. Macdonald

December 1978

Thesis Advisor: E.C. Crittenden, Jr.

SECURITY CLASSIFICATION OF THIS PAGE (When Data Entered)

REPORT DOCUMENTATION PAGE		READ INSTRUCTIONS BEFORE COMPLETING FORM
1. REPORT NUMBER	2. GOVT ACCESSION NO.	3. RECIPIENT'S CATALOG NUMBER
4. TITLE (and Subtitle) An Experimental System To Measure Atmospheric Extinction Of Visible, Near and Far Infrared Radiation In The Marine Boundary Layer		5. TYPE OF REPORT & PERIOD COVERED Master's Thesis December 1978 6. PERFORMING ORG. REPORT NUMBER
7. AUTHOR(s) J.R. Macdonald		8. CONTRACT OR GRANT NUMBER(s)
9. PERFORMING ORGANIZATION NAME AND ADDRESS Naval Postgraduate School Monterey, California 93940		10. PROGRAM ELEMENT, PROJECT, TASK AREA & WORK UNIT NUMBERS
11. CONTROLLING OFFICE NAME AND ADDRESS Naval Postgraduate School Monterey, California 93940		12. REPORT DATE December 1978 13. NUMBER OF PAGES 53
14. MONITORING AGENCY NAME & ADDRESS(if different from Controlling Office) Naval Postgraduate School Monterey, California 93940		15. SECURITY CLASS. (of this report) Unclassified 15a. DECLASSIFICATION/DOWNGRADING SCHEDULE

16. DISTRIBUTION STATEMENT (of this Report)

Approved for public release; distribution unlimited.

17. DISTRIBUTION STATEMENT (of the abstract entered in Block 20, if different from Report)

18. SUPPLEMENTARY NOTES

19. KEY WORDS (Continue on reverse side if necessary and identify by block number)

20. ABSTRACT (Continue on reverse side if necessary and identify by block number)

A method of measuring atmospheric extinction of radiation along a 13.3 kilometer path in the marine boundary layer has been devised and demonstrated. The design allows for selective measurement of extinction from the visible to the far infrared wavelengths. Two greybody sources, one covering the visible and near infrared and the other covering all bands out to the far infrared were each mounted on reflecting telescopes which

DD FORM 1 JAN 73 1473 EDITION OF 1 NOV 65 IS OBSOLETE
S/N 0102-014-6601

SECURITY CLASSIFICATION OF THIS PAGE (When Data Entered)

were used to project the radiation. A reflecting telescope with selectable detectors was employed as the receiver. Two feasibility trials were conducted and the equipment was successfully calibrated.

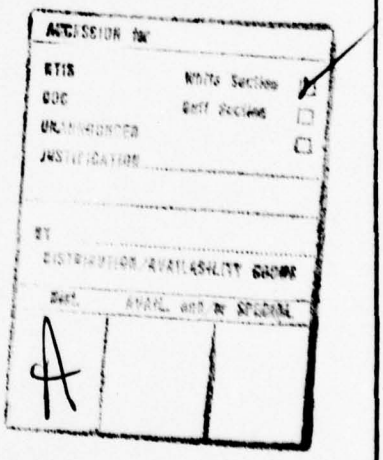

Approved for public release; distribution unlimited

(6) An Experimental System To Measure Atmospheric Extinction Of Visible, Near and Far Infrared Radiation In The Marine Boundary Layer.

by

(10) same
E.R. Macdonald
Lieutenant Commander, United States Navy
B.B.A., Saint Bonaventure University, 1965

(12) 54 p.

Submitted in partial fulfillment of the
requirements for the degree of

MASTER OF SCIENCE IN PHYSICS

from the
NAVAL POSTGRADUATE SCHOOL
(11) December ~~1978~~

(9) Master's thesis

Author: James R. Macdonald

Approved by: Eugene L. Crittendon Jr.
Thesis Advisor

Edmund A. Milne
Second Reader

W. M. Tolles
Chairman, Department of Physics and Chemistry

William M. Tolles
Dean of Science and Engineering

ABSTRACT

A method of measuring atmospheric extinction of radiation along a 13.3 kilometer path in the marine boundary layer has been devised and demonstrated. The design allows for selective measurement of extinction from the visible to the far infrared wavelengths. Two greybody sources, one covering the visible and near infrared and the other covering all bands out to the far infrared were each mounted on reflecting telescopes which were used to project the radiation. A reflecting telescope with selectable detectors was employed as the receiver. Two feasibility trials were conducted and the equipment was successfully calibrated.

TABLE OF CONTENTS

I. PROBLEM DESCRIPTION

A. GENERAL

The increasing development and deployment of electro-optical systems by the United States Navy Utilizing Foward Looking Infrared (FLIR), Lasers, Low Light Level Television (LLLTV) make it highly desireable to be able to predict the effect the atmosphere over the water has on the electromagnetic radiation being transmitted or received by these systems. Effects of the atmosphere on the radiation include scintillation, beam or image spread, wander, and extinction. Since the aerosol content of the atmosphere over the ocean varies significantly from over land, these effects also vary significantly from over land. Therefore, the objective of this thesis was to refine and demonstrate a technique to measure atmospheric extinction of infrared and visible radiation along a 13.3 kilometer path in the marine boundary layer.

Since 1971, an interdisciplinary group of professors at the Naval Postgraduate School have been pursuing research in a wide variety of electro-optic areas. Previous investigations by the group [1] and a number of thesis students have dealt with the investigation of the effect of atmospheric turbulence on the performance of imagers and beam projection systems. Some extinction measurements have been made using different laser sources. However, instabilities in the

lasers' amplitudes and output frequencies, particularly in the infrared, have made this method of data collection difficult. Therefore, the main sources used in this experiment were greybody radiation sources projected by reflecting telescope systems.

The data obtained from this experiment has application in two important areas. First, the extinction data obtained, along with large scale meteorological parameters, such as wind, humidity, visibility and temperature that were recorded at the same time, will be analyzed by the Naval Environmental Prediction Research Facility. The goal of this analysis will be the development of a prediction model of electro-optic system performance using only meteorological data as inputs. Second, the distribution of aerosol particle sizes will be measured along the optical path by use of Knollenberg nephelometers mounted on the Naval Postgraduate School research vessel Acania. Additionally, an aircraft from the Naval Ocean Systems Center (NOSC), San Diego, will be equipped with Knollenberg nephelometers and fly along the optical transmission path to collect aerosol particle spectra. From this data, a computer calculation will be made to predict extinction. Comparison of the computed and predicted results will allow verification of the computer models, allowing these models to be used in the design and technical testing of future electro-optical systems.

B. EXTINCTION - GENERAL

The atmosphere consists of a mixture of gases, mainly nitrogen, oxygen, carbon dioxide and water vapor, and aerosols, such as haze, fog, dust and rain. The gas molecules and aerosol particles cause extinction of the radiation through the processes of scattering and absorption. Scattering is the process by which a particle in the path of an electromagnetic wave continuously (1) abstracts energy from the incident wave and (2) reradiates that energy into the total solid angle centered at the particle [2]. The process can be explained in terms of electomagnetic wave theory. Briefly, the electric field of the incident or primary wave sets into oscillation the electric charges of the particle, be it a cloud droplet or molecule. The oscillating charges constitute one or more electric dipoles which radiate secondary spherical waves. The charges oscillate in phase with the primary wave and thus the secondary wave has the same frequency as the primary and bear a fixed phase relation to it. Scattering is a continuous process and when averaged over complete cycles produces no net change in the internal energy states of the particles. Spectrally, the process is also continuous, but is strongly dependent on wavelength for a given particle size.

While scattering produces no net change in the internal energy states of the particles, absorption causes a change in the internal energy and requires quantum theory for its

explanation. In a molecule, the internal energy is partitioned into rotational, vibrational, electronic and translational energy, with the first three quantized to discrete levels. The incident radiant energy is absorbed in quanta and the molecule undergoes a transition from a lower to a higher state of one of the three quantized interal energy forms. If, before the molecule can relax to the ground state and re-emit, molecular collisions occur, then non-radiating transitions can take place. In the case of thermodynamic equilibrium the energy is shared equally among all accessible internal energy states. When part of the energy is transferred to translational or kinetic energy, the process is called absorption [3]. This energy therefore causing a heating of the atmosphere.

The absorption in the atmosphere, mainly by carbon dioxide and water molecules is so great at certain frequencies that the atmosphere is practically opaque. Figure 1 from reference 4 shows a typical plot of transmittance of the atmosphere versus wavelength. From this plot, it can be easily seen why the three bands or "windows" from 0.5 to 1.06 micrometers, 3.0 to 5.0 micrometers and 8.0 to 14.0 micrometers have been used in visible and infrared systems. These windows will also be the area where the system decribed in the thesis will be optimized.

1. Mathematical Description

The fundamental law of extinction is attributed to

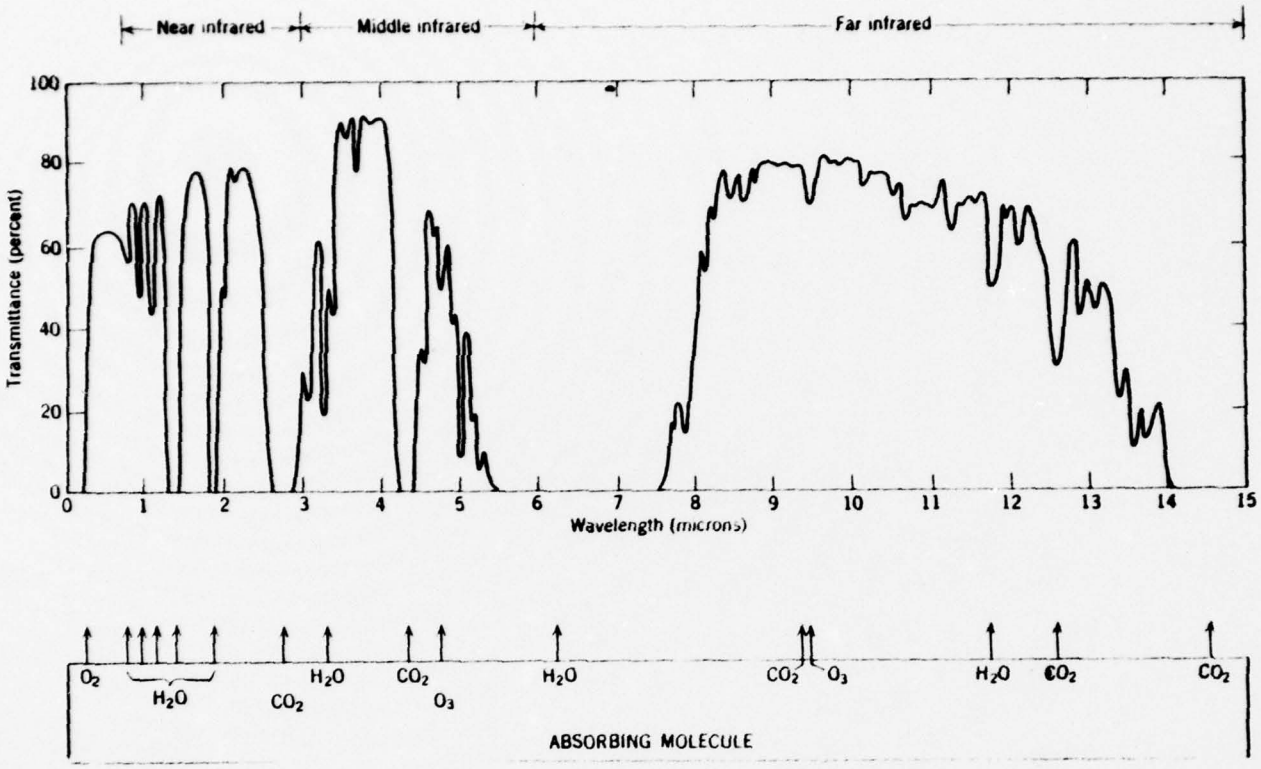

Figure 1. Typical Atmospheric Transmission and Absorbing Molecule Spectrum

both Bouguer and Lambert and relates the total scattering and absorption to the attenuation of the flux in a beam [3]. Considering the linear propagation of monochromatic radiation at frequency ν in a medium where the physical state (i.e., temperature, pressure and composition) is held constant, the law may be stated as follows:

$$(1)\quad F_x = F_o e^{-\mu x}$$

where

F_x = flux remaining after the beam has transversed a path length x

F_o = flux entering the attenuating layer

μ = extinction coefficient

x = path length in the attenuating layer

The extinction coefficient can be expressed as the sum of the coefficients for total absorption and for total non-forward scattering.

$$(2)\quad \mu = \sigma_{absorption} + \sigma_{scattering}$$

Furthermore, since the molecules and aerosols enter into the scattering and absorption processes, absorption and scattering may be subdivided as shown below

$$\sigma_{ab} = k_m + k_a$$

$$\sigma_{sc} = \sigma_m + \sigma_a$$

where

k_m = molecular absorption coefficient

k_a = aerosol absorption coefficient

σ_m = molecular scattering coefficient

σ_a = aerosol scattering coefficient

The use of a reflecting telescope system to project the source means that the source output is in the form of spherical waves, vice plane waves. Therefore, the inverse square law [5] for spherical wave fronts is taken into account by writing

$$E_x = \frac{E_o e^{-\mu x}}{\Omega x^2}$$

and

$$E_x = \frac{L_o e^{-\mu x}}{x^2}$$

where

E_x = irradiance or flux per unit area of source in watts per square centimeter at a distance x

E_o = irradiance in watts per square centimeter at source

L_o = radiance or flux per unit area of source per unit solid angle

Ωx^2 = area of beam at distance x

If we make a calibration measurement at a short range, x_c, where the beam is diverged sufficiently to insure complete coverage of the collecting aperture by the beam, then

$$E_c = \frac{L_o e^{-\mu_c x_c}}{x_c^2} \approx \frac{L_o}{x_c^2}$$

if the calibration range conditions are such that the extinction coefficient μ_c is small so that $\mu_c x_c \approx 0$.

Then

$$(3)\quad L_o = E_c\, x_c^2$$

so $$E_x = \frac{E_c x_c^2 e^{-\mu x}}{x^2}$$

Letting

$$T = \frac{E_c\, x_c^2}{E_x\, x^2}$$

Then

$$T = e^{-\mu x}$$

$$\ln T = -\mu x$$

and $$= (\ln T)/x$$

The assumptions and limitations of this procedure are

1. μ is not a function of x.
2. The flux that is scattered forward is not accounted for in Bouguer and Lambert's Law.
3. μ_c is small at the time of calibration.

The requirement that the beam at the calibration distance be diverged sufficiently to completely cover the receiving aperture means that the source telescope focus has to be changed for the calibration measurement. The image of the source is focused on the receiving telescope aperture for both the 13.3 km and .360km measurements. This change in focus does not affect the experimental data since the radiance of an image equals that of the object regardless of magnification. This assumes that there are no atmospheric losses or optical losses and is proved below.

Figure 2 shows a lens forming the image dA' of a surface element dS of the object. The radiant flux dF entering the receiving aperture is limited by the area dA" of the detector so that only the narrow bundle indicated by the broken lines contribute to the image on the detector. Now the flux flowing from a point on dS within the small solid angle subtended by the element of area dA at the distance r is proportional to the solid angle. This is found by dividing the area of dA projected normal to the rays by r^2 so that the radiant flux can be written as

$$dF = \text{constant } \frac{dA\cos\phi}{r^2}$$

Our source is of finite size so we must consider all points on dS to emit flux. Since our source is also a "Lambert Law radiator" the flux will be proportional to the projected area of dS so that

$$dF_{exit} = \text{constant } \frac{dA\cos\phi\cos\theta ds}{r^2}$$

The constant depends only on the source and is called the radiance (L) and has units of watts per unit area per steradian. The radiant flux incident per unit area on the lens can now be expressed as

$$\frac{dF}{dA} = \frac{L\cos\theta dS\cos\phi}{r^2} = dE$$

where dE is the irradiance in watts per unit area.

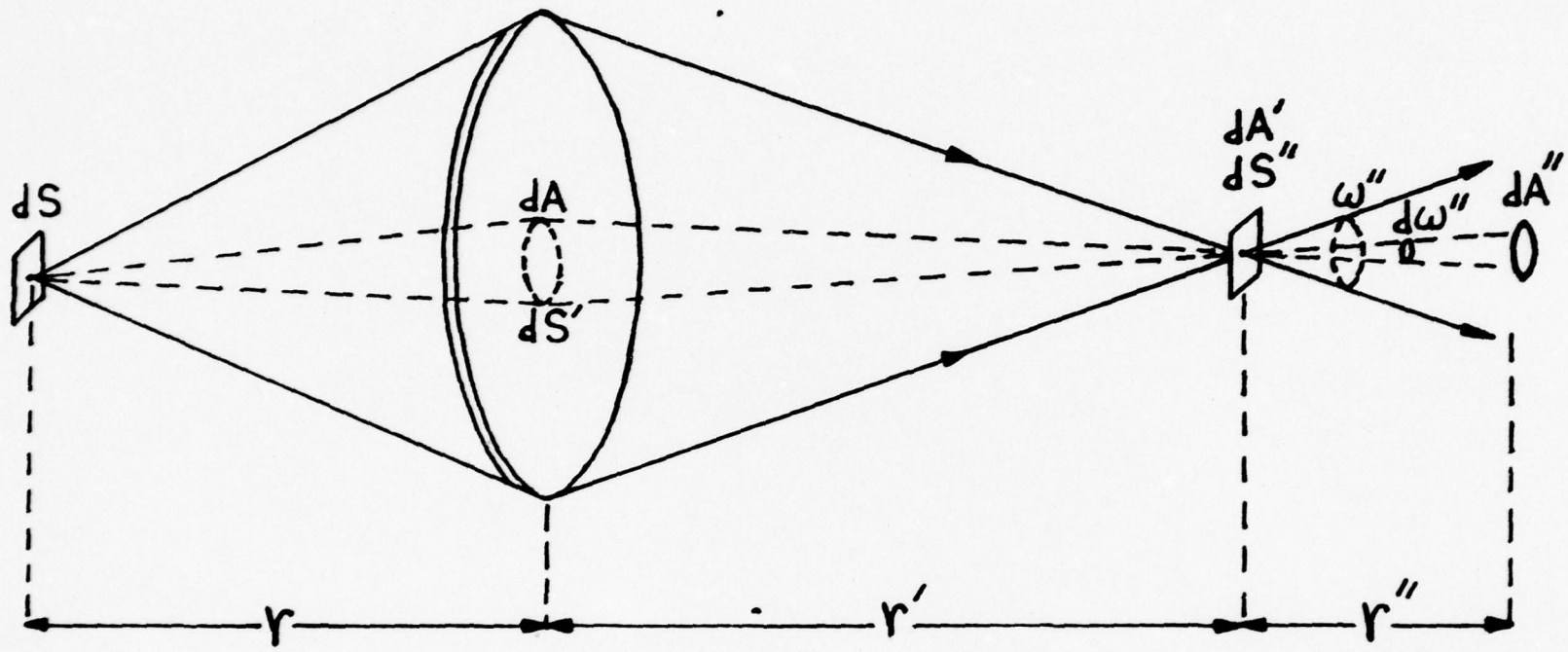

Figure 2. Geometry for Treating Image Brightness

Now since the quantity dF remains constant for a bundle of rays as it traverses an optical system [5],

$$\frac{dF}{L} = \frac{dAdS\cos\theta\cos\phi}{r^2} = \frac{dA'dS'\cos\theta'\cos\phi'}{(r')^2} = \frac{dA''dS''\cos\theta''\cos\phi''}{(r'')^2}$$

The last term of the equation refers to a bundle of rays in the region to the right of the image, and since the flux in the bundle is assumed not to be attenuated, we have

$$\frac{dF}{L} = \frac{dF}{L''}$$

where L'' denotes the radiance of the image.

Hence L = L'' and there is no restriction on the position of the object in relation to the focal point of the system. Therefore, the magnification is not important as long as the image at least fills the receiving aperture.

II. EXPERIMENTAL PROCEDURE

A. GENERAL

The experimental instrumentation consists of four radiation sources (2 gray bodies and 2 lasers) and one receiving telescope with selectable detectors for the various wavelengths of interest. The radiation sources are mounted on the covered bed of a 2½-ton truck which was parked at the Marina Sewage Plant. The location is approximately 60 feet above sea level and 450 feet from Monterey Bay. The receiving instrumentation was located in the United States Coast Guard fog horn building at Point Pinos. The building is approximately 15 feet above sea level and 500 feet from Monterey Bay. Figure 3 and 4 contain photographs of the truck and fog horn building while Figure 5 show the overall geographic location of the installations. The optical path between the sources and receiver was measured to be 13.3 kilometers long by use of Coast and Geodetic Survey Chart, similar to the one shown in Figure 5.

The requirement to calibrate the system at a short range was met by moving the truck containing the sources to a parking area in front of the Point Pinos Lighthouse, located 360 meters from the fog horn building. The receiving optics were rotated and elevated to allow line of sight between receiver and source. The path length, which was measured with steel measuring tape to be 360 meters

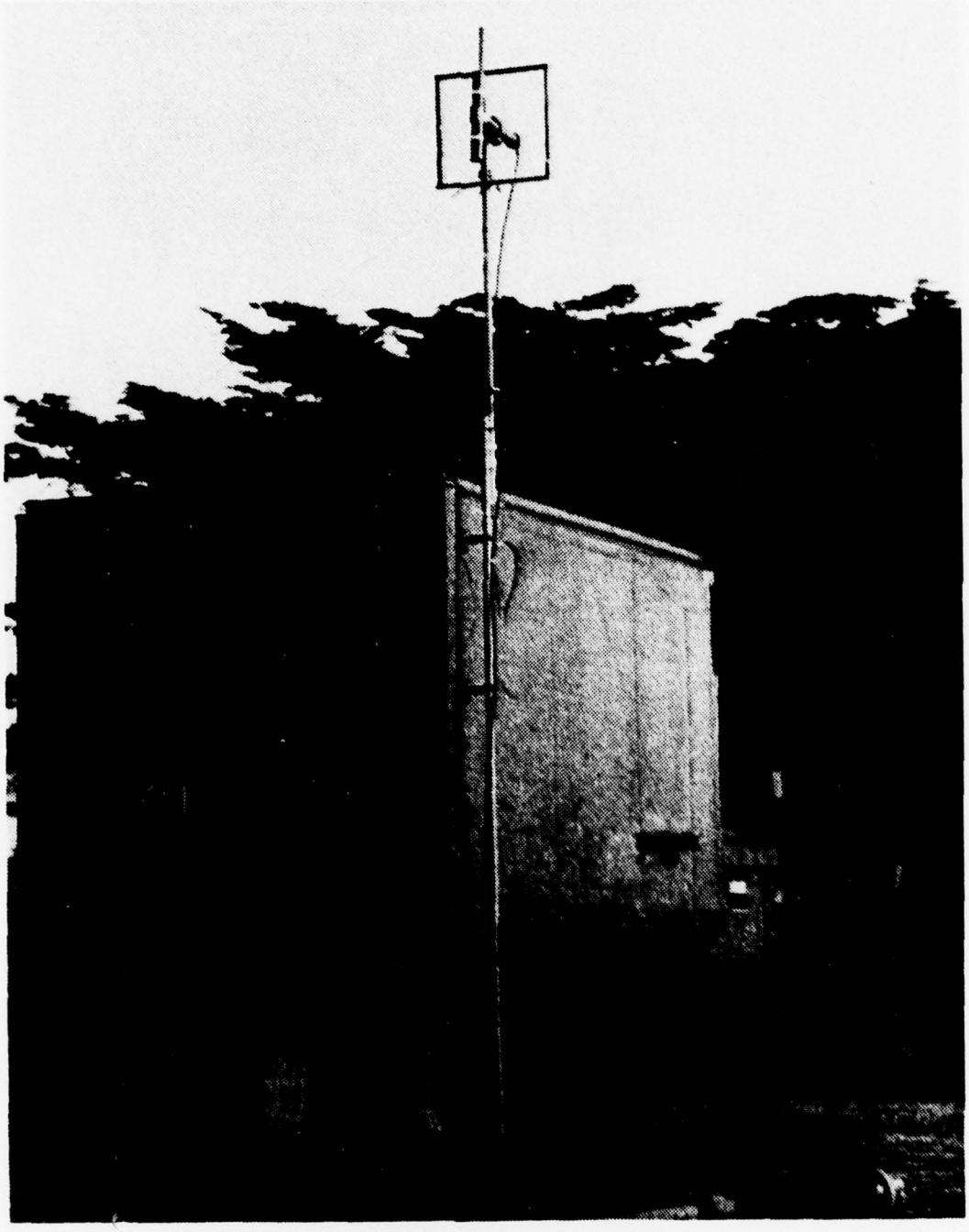

Figure 3. Truck Containing Sources Positioned at Calibration Site

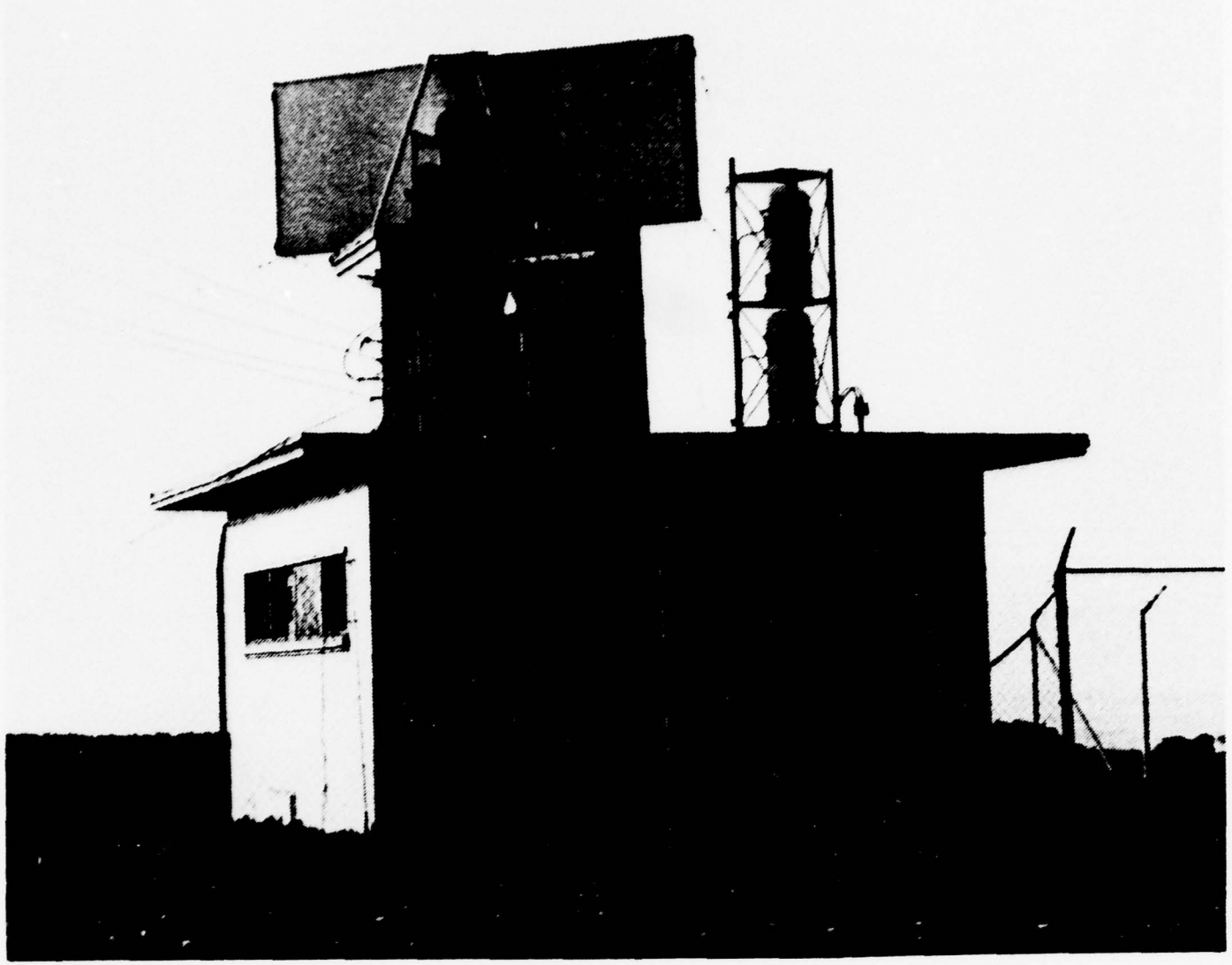

Figure 4. Point Pinos Fog Horn Building

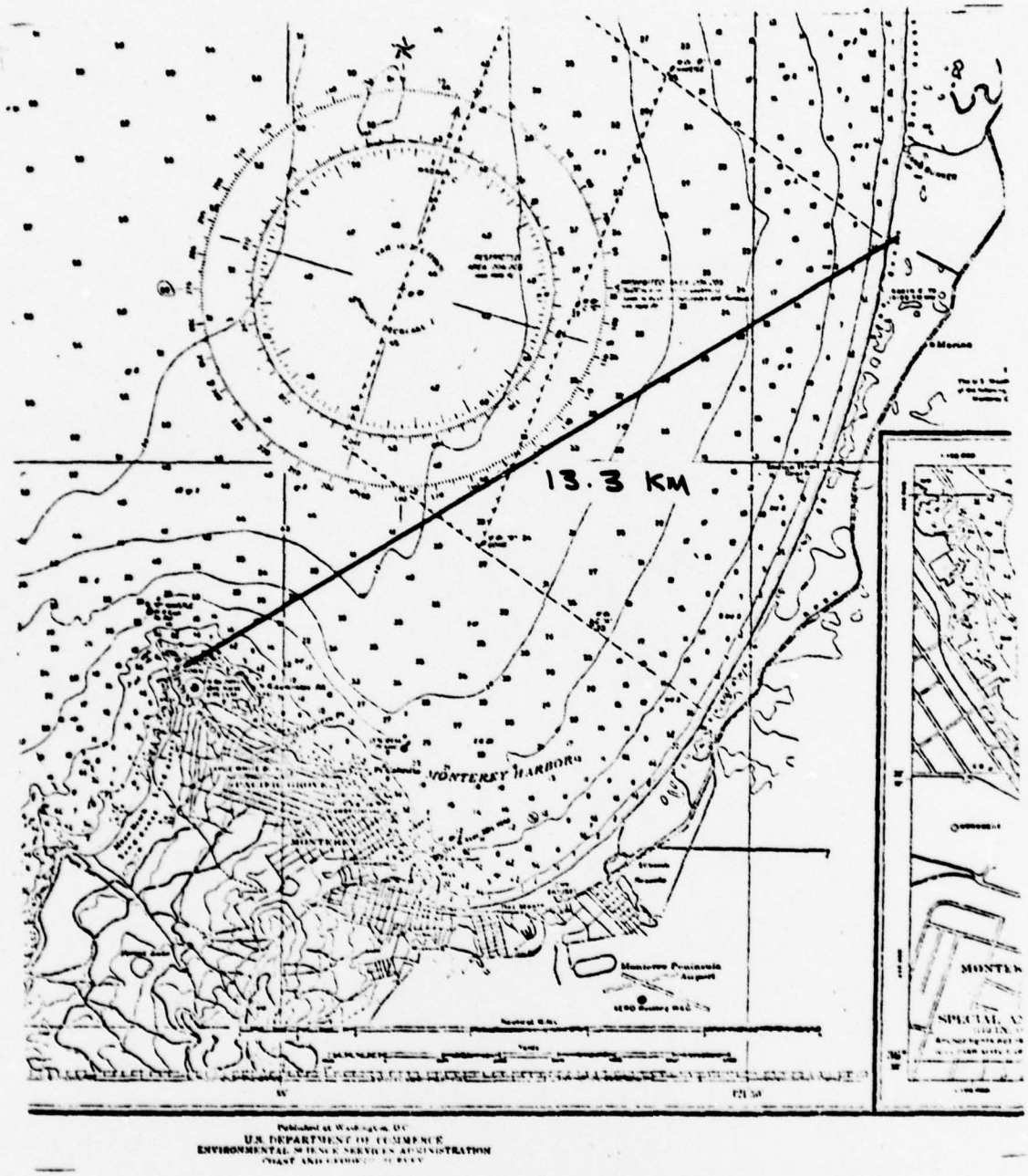

Figure 5. Optical Path Across Monterey Bay

passed over ground covered with either ice plant or grass.

B. DETAILS OF TRUCK MOUNTED EQUIPMENT

1. Truck Mounted Equipment

Equipment described in the following paragraphs is mounted on the bed of a 2½-ton truck. The greybody and laser sources are mounted on a platform that is supported by four hydraulic camper jacks. The jacks are extended through holes in the floor to the ground, providing a stable mount for the sources and isolating them from any vibrations of the truck. Electrical power for the equipment is provided by extension cord from the sewage plant. The truck is elevated by ramps and jacks 10 inches to insure the optical path is not interrupted by a security fence that surrounds the sewage plant.

a. Greybody Source #1

The primary greybody radiation source is a metallic ribbon filament enclosed in a ceramic case and operated in the open atmosphere to insure transmission of the long wavelength infrared. The source is the type used in the Perkin Elmer Model 137B Spectraphotometer and approximates a greybody out to 15 micrometers. The radiating ceramic case is three millimeters in diameter and 5 millimeters long. Power to operate the source is provided by two Hewlett-Packard 15 ampere direct current power supplies operated in parallel. Directly in front of the source is

mounted a chopper driven by a variable speed AC motor. The chopper, consisting of a circular wheel with 16 slots, was designed to provide a 50% duty cycle. The RPM of the chopper was varied to provide a square pulse signal output at approximately 920Hz.

The source is operated at a temperature of 1800°K, a temperature that was measured in the laboratory using a Leeds and Northrup Model 8632-C pyrometer. The measurement was made with the chopper operating and the pyrometer reading was corrected for the combined emissivity of the aluminum chopper and source. The voltage and current of the source at this temperature were recorded and these parameters were used to set the source at the desired operating point.

The source and chopper are attached to an adjustable mount and attached to the side of an 18 inch modified Dall-Kirkham reflecting telescope (Figure 6). The primary mirror is eliptical while a Newtonian flat is used as the secondary mirror. The Newtonian flat, vice a spherical secondary, is used to reduce the equivalent focal length of the telescope from 256 centimeters to 163.2 centimeters. This reduction allows increased magnification of the image and insures that the image will more than fill the collecting aperture at 360 meters. The telescope assembly is fastened on an adjustable mount which allowed precise adjustments in the horizontal and vertical directions

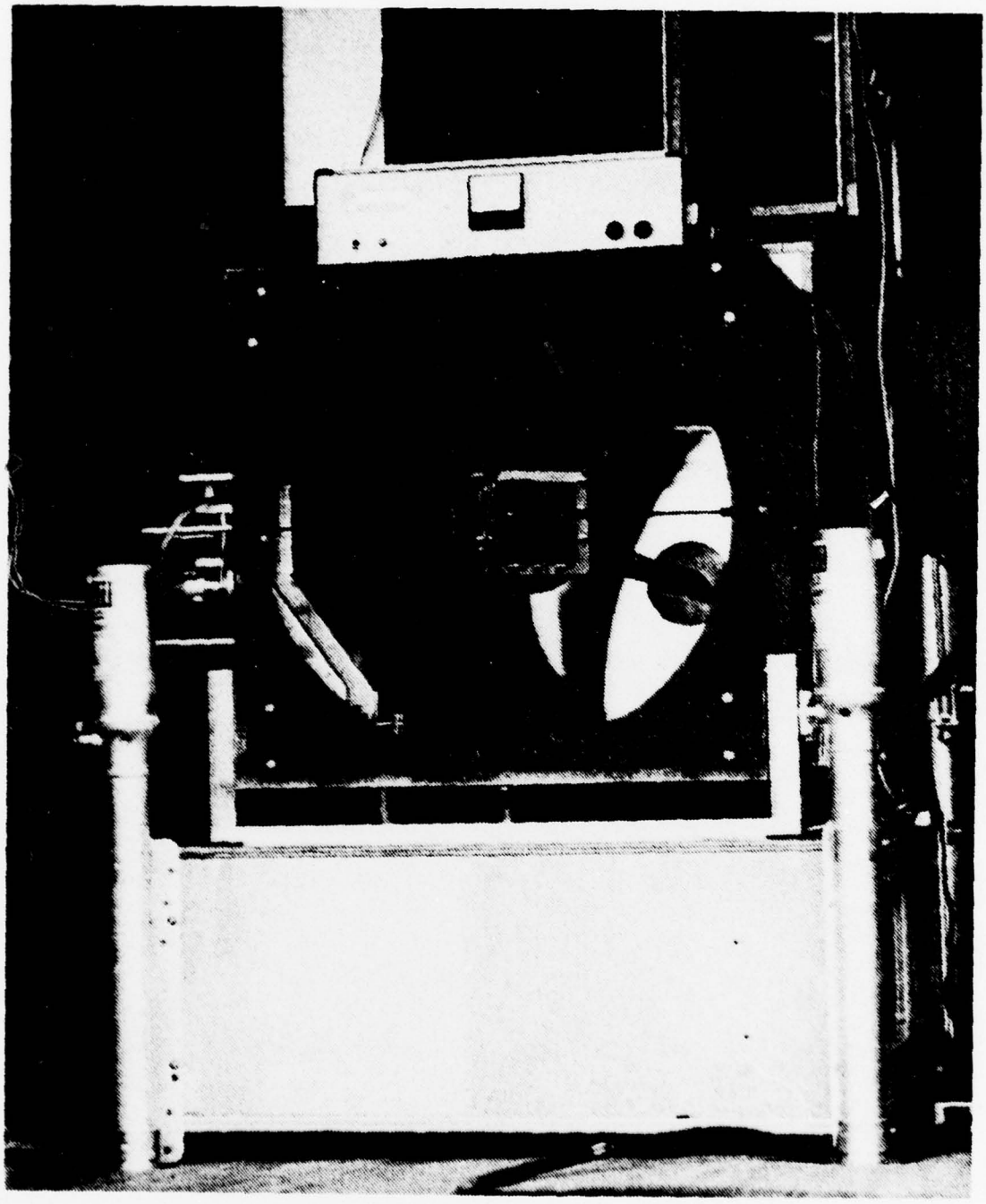

Figure 6. Greybody Source #1

by use of screw jacks.

b. Greybody Source #2

The second greybody source is a tungsten ribbon filament enclosed in a glass case. This source, which was calibrated in the same manner as the first source, was operated at a temperature of 2800°K and acted as a greybody out to approximately three microns. The glass enclosure serves as the frequency limiting component of this source. The six volts and 16 amperes required to operate it were supplied by the same power sources as greybody #1. The source, along with a variable speed chopper, is mounted on the side of a 10 inch diameter modified Dall-Kirkham reflecting telescope (Figure 7). An aluminum case with a 100 cubic feet per minute fan mounted on one side is used to enclose the source and chopper (not shown in Figure 7). The fan is required to cool the chopper motor which is located directly above the source.

The telescope contains a perforated ellipsoidal primary mirror and a Newtonian flat secondary, and has an effective focal length of 98.2 centimeters. The Newtonian flat is used instead of a spherical secondary for the same reason as for greybody #1. The chopper is a 20 slotted circular aluminum wheel with a 50% duty cycle. It is driven by a variable speed DC motor to provide a signal output frequency of approximately 920Hz. The telescope has an adjustment mechanism that allows adjustment in the horizontal

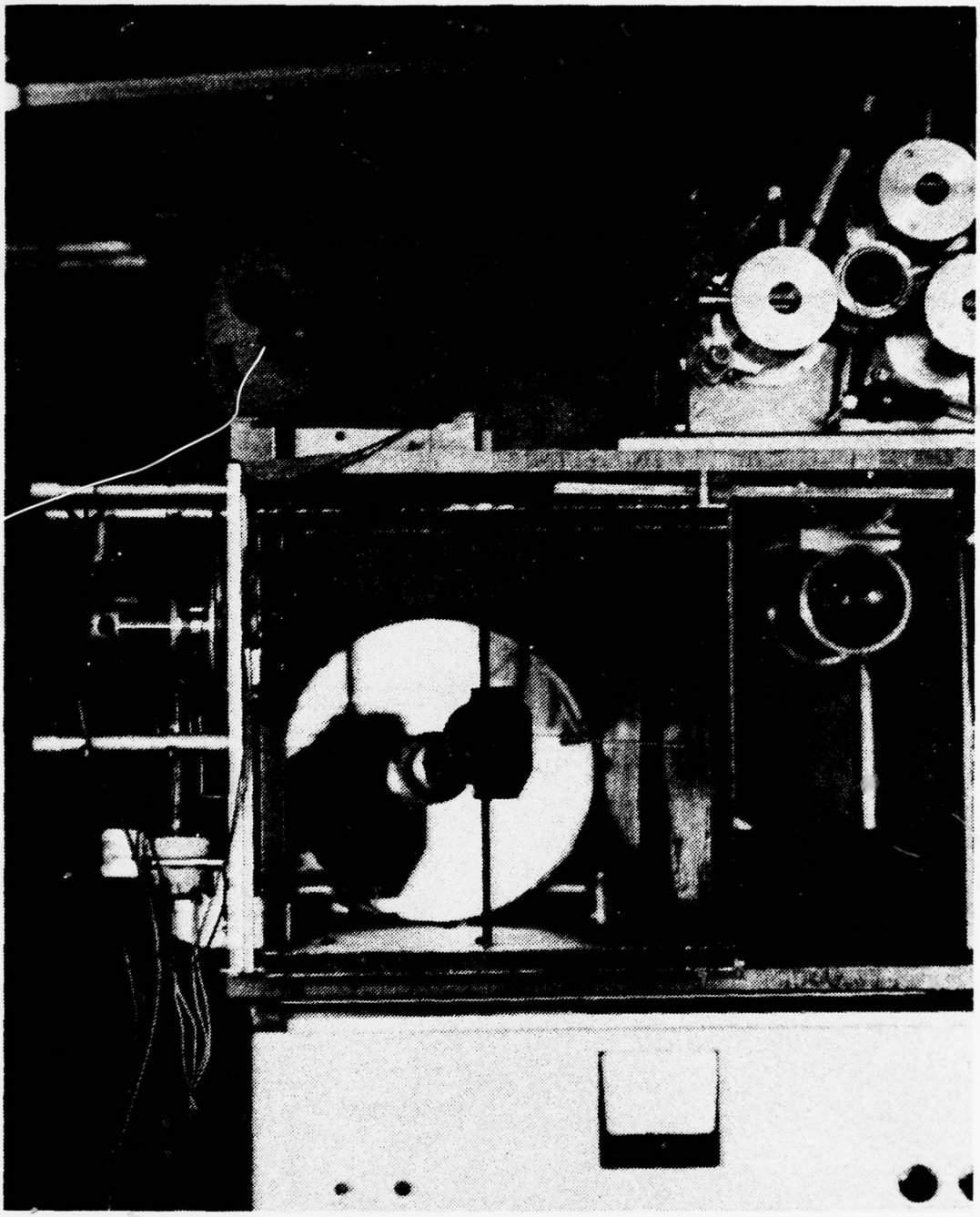

Figure 7. Greybody Source #2

and vertical directions. The entire structure, consisting of the telescope and mount is placed on top of the #1 greybody telescope.

The second greybody source was used to provide a larger flux in the visible and near infrared regions. Referring to Figure 8, the change in the radiance at .49, .63 and 1.06 micrometers is at least a factor of ten when changing from 1800°K to 2800°K assuming both greybodies have the same emissivity. Since the irradiance of the image is proportional to the product of the radiance of the source and the area of the exit pupil 5 , the 10" telescope's radiance is approximately 30% of the 18" telescope's radiance. Therefore, an average overall increase in the signal received at the detector of 3 times the 1800°K greybody signal was expected.

c. Laser Sources

Two laser sources are mounted on the top of Greybody #2's telescope. One is an Argon ion laser transmitting at .4880 micrometers (blue) and the other is a HeNe laser emitting at .6328 micrometers (red). They will not be discussed further as the scope of this paper only includes the greybody source experimental procedures.

d. Source Intensity Monitor and Trigger Mechanism

A United Detector Technology Corporation Pin 6D photodiode is mounted in the opening in the center of the primary mirror of both greybody source telescopes.

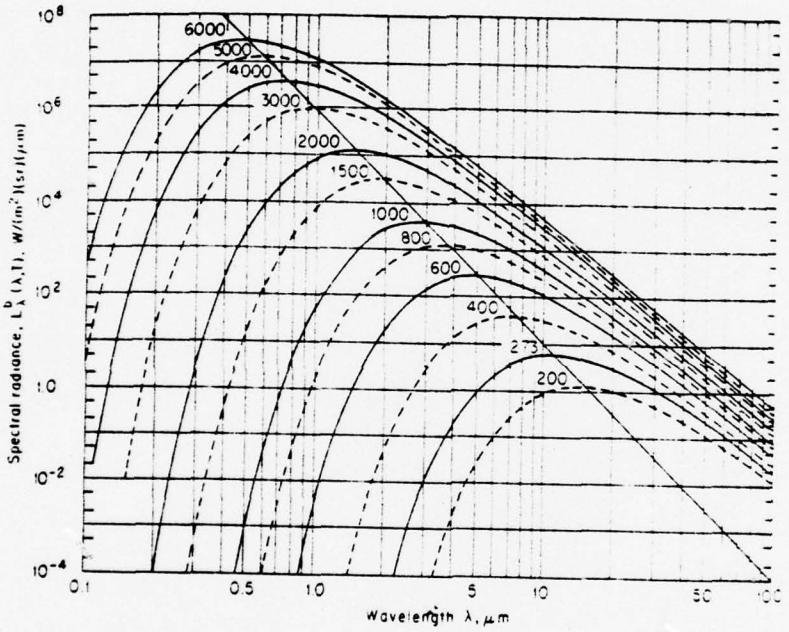

Figure 8. Spectral Radiance L of a Blackbody at the Temperature in Kelvin. Subdivisions of the Ordinate Scale are at 2 and 5 [Ref 6]

The diode, operated in the photoconductive mode by baising at 22½ volts, is mounted in a case with a thermally controlled environment and is used to monitor the source output radiance. Mounted on the optical axis of the telescope, it receives the center portion of the outgoing radiation. The output of the detector is fed to a PAR 113 low noise differential preamplifier having gain ranging from 10 to 10^4. The PAR 113 additionally has adjustable high and low frequency rolloffs allowing appropriate bandwidth selection.

The output of the PAR 113 is displayed on a Thornton 4010 Oscilloscope. The output of the photodiode was considered to be the calibration point for setting the source radiance. The output of the PAR 113 is sent to a demodulator circuit which samples the peak signal. The average is read on a Hewlett-Packard 3476A digital voltmeter. The photocell output pulses, which have been amplified by the PAR 113, are also used to trigger an Interstate Electronics Corporation P12 pulse generator which generates a 100 microsecond trigger pulse corresponding in time to the leading edge of the detector pulse. This trigger pulse is then used to trigger the Thornton Oscilloscope while simultaneously being displayed on the scope. The trigger pulse is additionally sent to a UHF transmitter operating at 256.2 megacycles. The transmitter has an output of 3.5 watts, and is connected by RG-59B coaxial cable to a U.S. Navy AT-150/SRC coaxial dipole antenna mounted on a 20 foot

high pole. A screen mesh flat plate reflector is mounted behind the antenna to increase the antenna gain by approximately 2.5 dB over an isotropic antenna. A block diagram of the above signal flow is shown in Figure 9.

2. Fog Horn Building Equipment

The equipment described in the following paragraphs was located in the Point Pinos fog horn building. The building is located approximately 15 feet above sea level and 450 feet back from the shore line along the optical path. The land between the building and the shore line consists of sand dunes, ground covered with ice plant and a two-lane asphalt secondary road. Prior to the start of the experiment a gate structure was placed in the security fence that surrounds the building. This allowed an uninterrupted optical path between the doors of the building and the truck located at Marina. For calibration, the receiver was rotated and elevated to align with an opening that was made in one wall of the building. This allowed an uninterrupted optical path between the receiver and the truck which was located 360meters away when calibrating the system.

a. Receiving Optics

The receiving system consists of an 45.72cm diameter modified Cassegrainian telescope with a paraboloid primary mirror and a convex hyperboloid secondary. A flat elliptical mirror is mounted at 45° to the axis in the 12.7cm

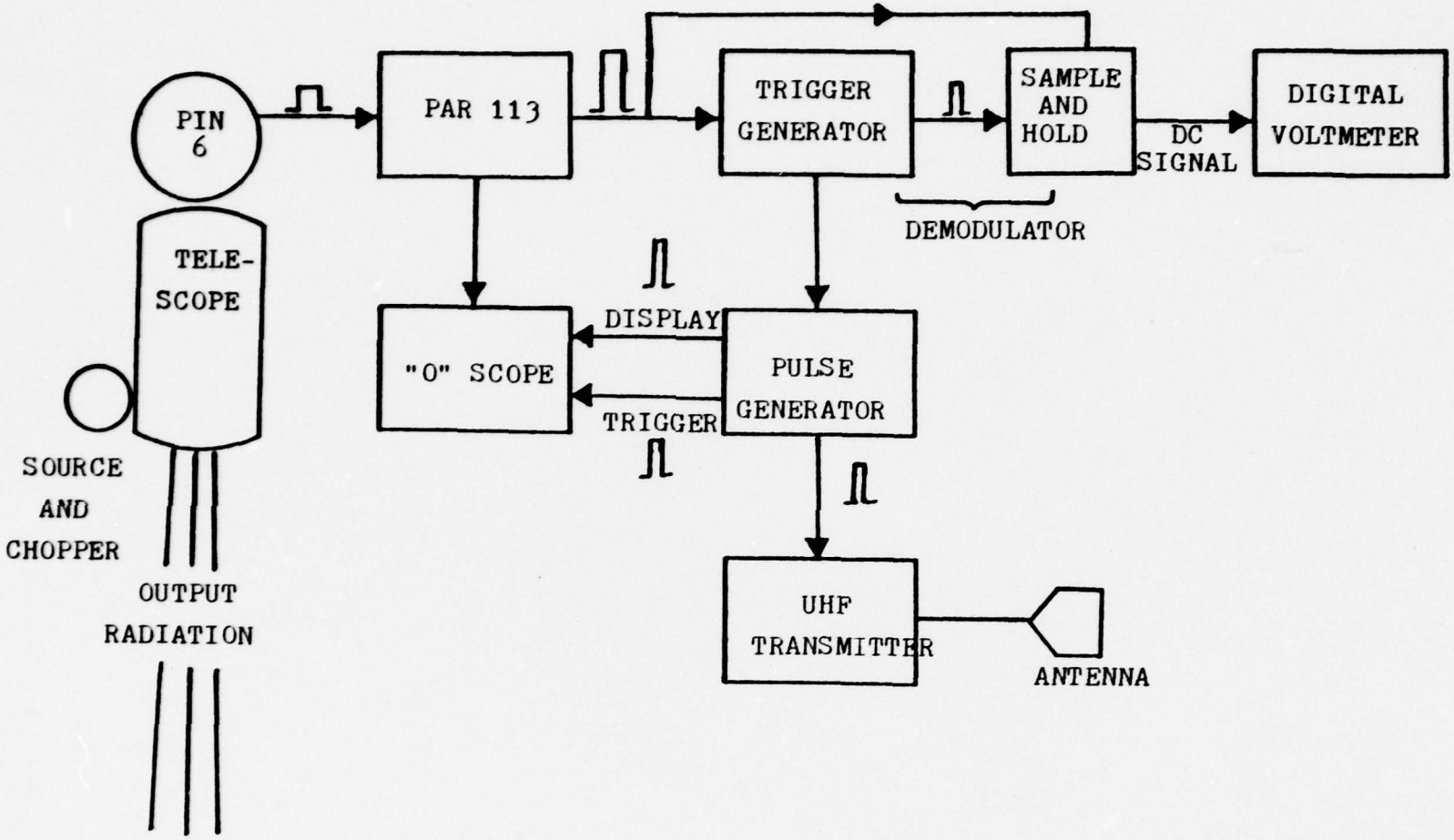

Figure 9. Source Intensity Monitor and Triggering Circuit

diameter hole in the center of the primary mirror, thus placing the focus on the side of the telescope. The radiation reflected by the elliptical flat is directed to one of the four detectors that are mounted on an arm extending from the side of the telescope (Figure 10). A precisely adjustable mirror is used to direct the radiation 90^{o} to the detector selected for use. Each arm that holds a detector is internally threaded and painted black to reduce the amount of scattered light incident on the detector. Additionally, a pin-hole spatial filter was added in the focal plane which blocks some of the scattered radiation and the radiation from the region surrounding the source. The optical bandwidth defining filter was placed just beyond the pin hole. Finally, a field lens was placed just beyond the bandwidth filter. The field lens forms an image of the entrance aperture of the system, so the distribution of the radiant flux across the detector is not affected by changes in pointing of the receiving telescope, provided the entire source remains in the receiver field of view. The field lens is germanium for the middle and far infrared detectors and glass for the visible and near infrared wavelengths.

The entire telescope and detector assembly is attached to an adjustable mount that allows precise alignment of the telescope in the horizontal and vertical directions through the use of screw jacks. The mount is

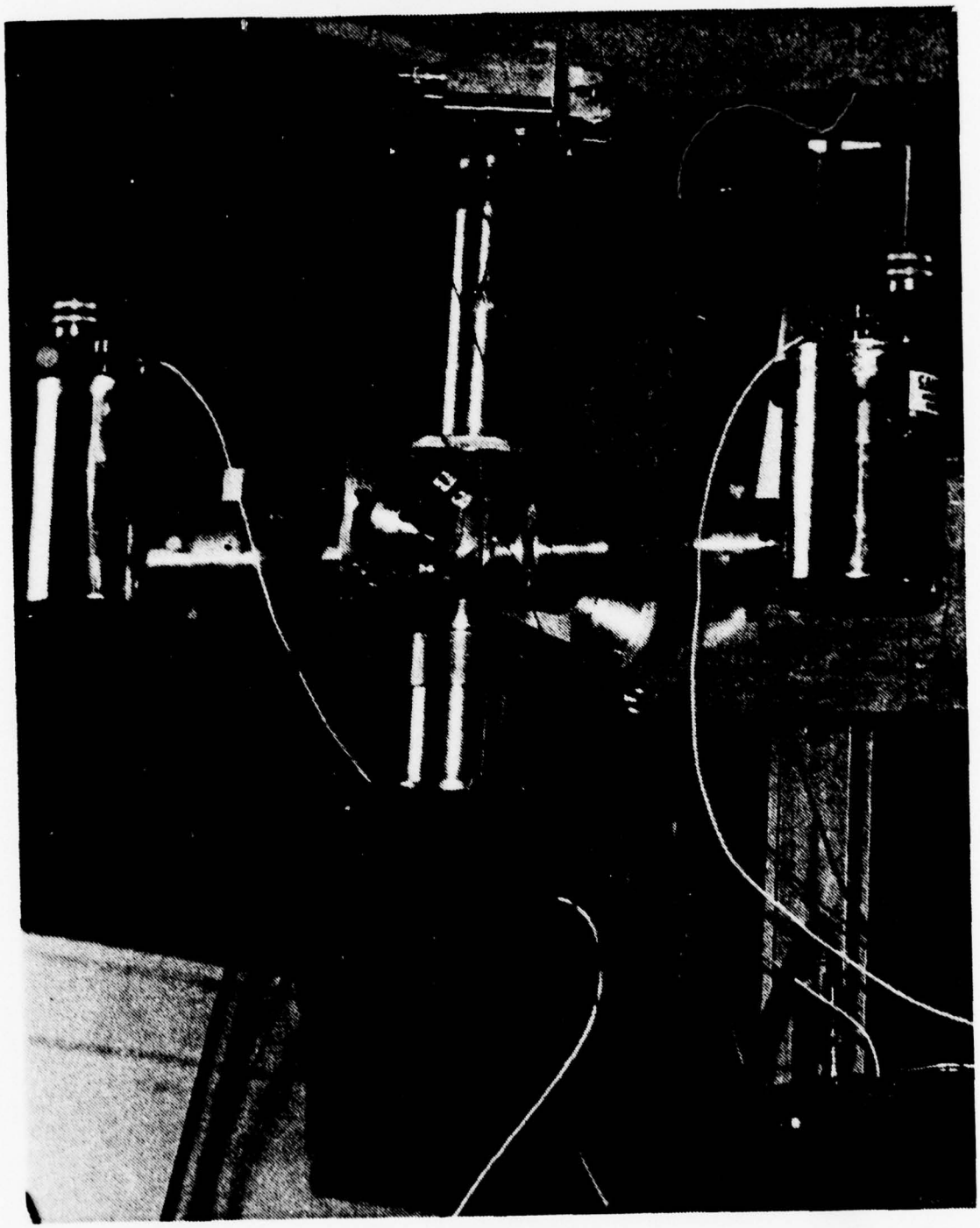

Figure 10. Detector Mounting Apparatus

supported on two concrete tables (Figure 11) to isolate the receiver from vibrations caused by personnel walking near the telescope or from the wind blowing against the telescope. An eight power spotting scope is mounted atop the telescope and used for the initial rough alignment with the sources.

b. Silicon Detector

A General Electric silicon avalanche multiplier detector with a diameter of two millimeters is used to detect signals in the visible and near infrared. A bias voltage of 2000 volts is provided to achieve an internal gain of 50. A field effect transistor is used to provide an impedence match between the dropping resistor and the output cable. A rotary switch allows selection of various dropping resistors to enable choice of best signal-to-noise ratio. The detector assembly is constructed to allow rapid change of interference filters. Filters used with the silicon detector allow detection at .4880, .6328 and 1.06 micrometers, and had a one-half height bandwidth of .010 micrometers. Figure (12) shows the location of these bandwidths in comparison with the atmospheric transmission curves. The detector was operated at a fixed temperature of 25°C. The detector and resistor array are mounted in aluminum box enclosed within an insulated heat shield. The interior is heated by a resistive heater. The temperature is monitored by a pin-head size "Thermistor" element whose resistance as a function of temperature is known. The

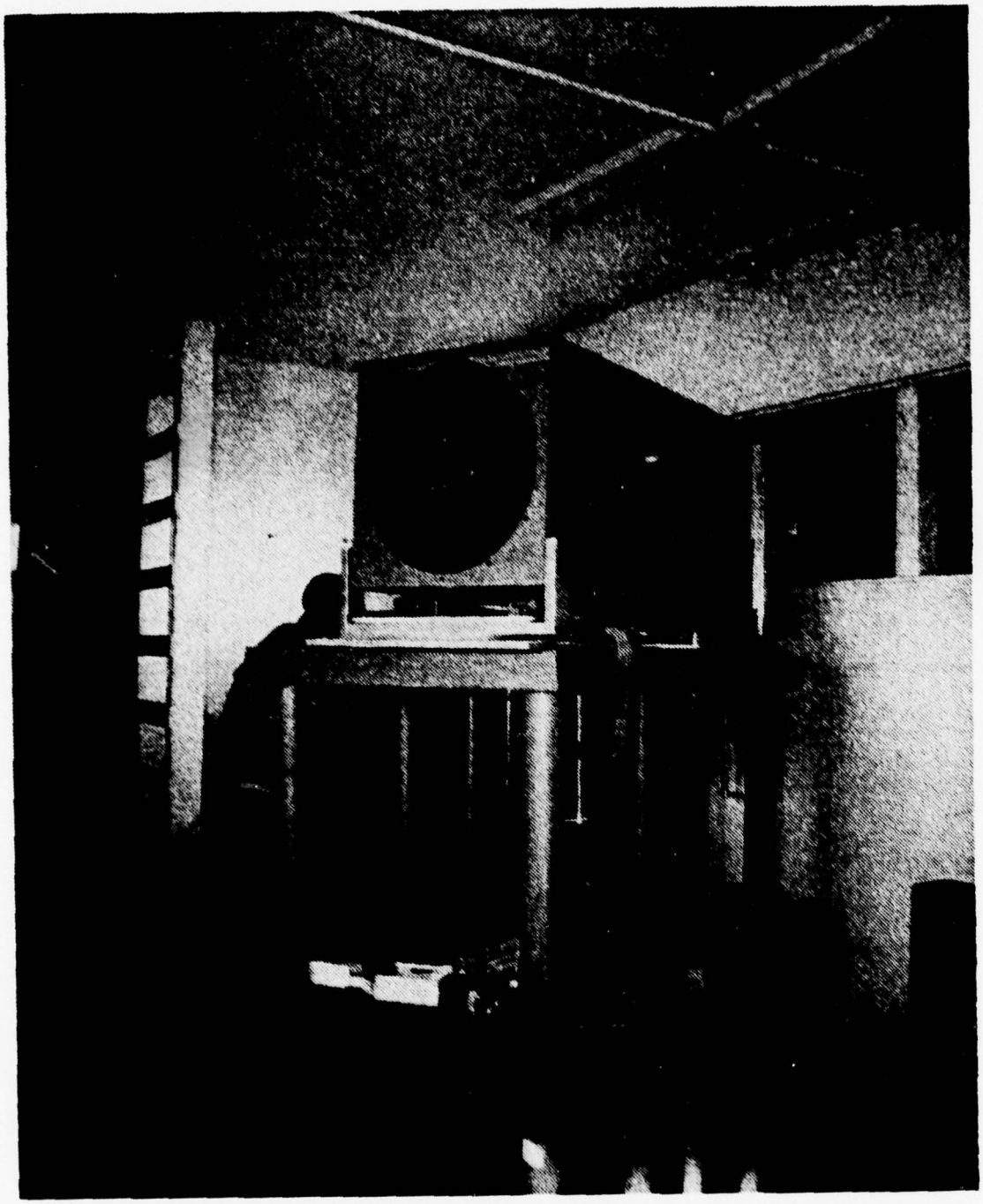

Figure 11. Receiving Telescope Positioned For Calibration

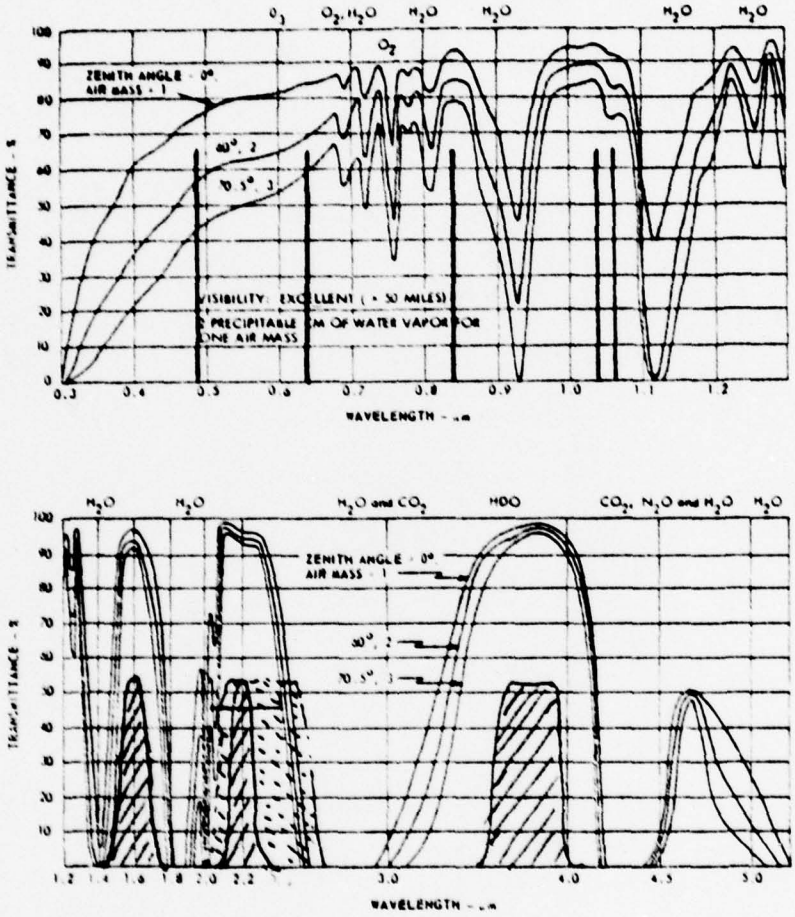

Figure 12. Bandpass regions for greybody source filters, superposed on curves of atmospheric transmission for paths through the complete atmosphere at varying zenith angles. The vertical path is the equivalent of about 8km horizontal path at sea level.

desired temperature is maintained by manually controlling the heater voltage input.

c. Germanium Detector

A Judson Infrared Corporation photovoltaic photodiode is used to detect 1.60 micron radiation Figure 12 . A filter with a one-half height bandwidth of .112 micrometer, centered at 1.6 microns, was placed in the detector tube along with a glass field lens. The photodiode is operated in the photoconductive mode by providing a .15 volt back-bias to the cell. A rotary switch allows determination of best signal-to-noise. At the calibration distance, a low dropping resistance was required to insure the output signal was not saturating the PAR 113. The detector was operated at a fixed temperature of 25°C by the same process as described in the preceding paragraph on the silicon detector.

d. Indium-Antimonide Detector

A 2.0 millimeter diameter indium-antimonide photo-voltaic detector located behind a non-reflection coated silicon window is used to detect 2.25 and 3.8 micrometer radiation (Figure 12). The detector, manufactured by the Santa Barbara Research Center is enclosed in a dewar since it requires cooling to 77°K for optimum performance. The dewar insulating region is evacuated to 10^{-6} Torr and the dewar filled with liquid nitrogen prior to use. Two bandpass filters, one with a one-half height bandwidth of

.30 micrometers centered at 2.25 micrometers and the other with a .30 micrometers bandpass centered at 3.80 micrometers are arranged for rapid insertion in the detector monitoring arm. A germanium field lens is located just behind the filter.

e. Mercury-Cadmium-Telluride Detector

A 2.0 millimeter square mercury-cadmium-telluride photoconductive detector, located behind an Irtran II window, is used to detect 10.66 micrometers radiation (Figure 13). The detector was manufactured by the Santa Barbara Research Center and is enclosed in a dewar since it requires cooling to 77°K for optimum performance. The dewar insulating region was evacuated to 10^{-6} Torr and the dewar filled with liquid nitrogen prior to use. A bandpass filter which had a one-half height bandwidth of 2.85 micrometers and centered at 10.66 micrometers is located in the detector mounting arm along with a germanium field lens. The measuring current is provided by a 6 volt dry cell applied to the detector in series with a 190 ohm resistor as a current limiter. The cell voltage drop is detected as the signal.

f. UHF Receiver

The trigger signal broadcast from the truck is received using a locally manufactured helix antenna that is optimized to receive 256.0 megahertz (Figure 14). The antenna is mounted on the roof of the fog horn building and has an approximate gain of 5dB over an isotropic antenna.

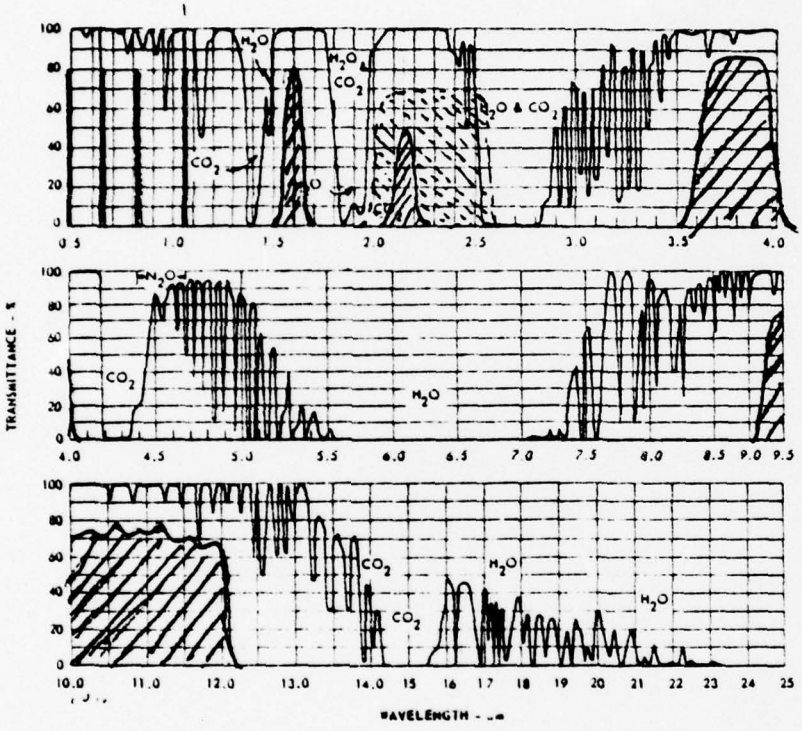

Figure 13. Bandpass regions for greybody source filters, superposed on curves at atmospheric transmittance for a 1000 ft. path at sea level containing 5.7mm of precipitable water at 79°F.

Figure 14. UHF Helix Trigger Receiving Antenna

The received signal is sent to a UHF broadband FM receiver where the signal is demodulated. The demodulated signal is displayed on the Um 328 Oscilloscope and used to provide a timing pulse for the NIC 80 computer which is described in the next paragraph.

g. Signal Processing

The output of all four detectors is routed through a switching unit which allows selection of a single detector output to be processed. The signal is amplified by a PAR 113 amplifier and then routed to a computer terminal, consisting of a Hewlett Packard 9825A and a Nicolet Instrument Company NIC-80, which consists of a 12,000 20-bit word digital computer and a Tektronix CRT display, digitizes the analog input signal and performs the required data processing functions. The Hewlett Packard 9825A acts as an output device for the NIC-30 with the ability to provide a real time printer readout of the output data. Appendix A provides a description of the method employed to calculate the actual extinction coefficient.

III. THE EXPERIMENT

A. INITIAL SETUP AND ALIGNMENT

The initial testing of the sources and receiving units was performed in the basement hallway of Spanagel Hall, Naval Postgraduate School (NPS). The sources and detectors were located at opposite ends of the hallway, a distance of 430 feet. The receiving telescope was focused on the exit aperture of the source telescope while the source telescopes were focused on the focal plane of the receiving telescope. Alignment was accomplished by scanning the receiving telescope in the horizontal and vertical directions to set the position in the center of the flat topped response. The source was then scanned until positioned in the center of the flat topped response. Finally, each detector was varied in position until positioned in the center of the flat topped response. This final process was aided by an up/down and left/right set of adjustments for each field lens. This complete adjustment process was repeated until a signal was received at the detector that was uniform as the telescope alignment was varied.

B. UHF TRIGGER SIGNAL TESTS

The capability to transmit and receive a trigger signal at 256.2 megacycles was reached after two unsuccessful attemps using various UHF antennas. The successful configuration resulted when a flat plate reflector was added to a

previously tried dipole antenna and the entire structure elevated 20 feet by use of a pole attached to the 2½ ton truck. The second antenna used was a helix antenna specifically designed to operate around 256.0 megacycles.

C. FEASIBILITY TRIALS

Two different feasibility trials were then conducted to verify that the experimental system could detect the transmitted signal at 13.3 km. The first trial was conducted at night to facilitate initial lineup of the telescopes. A Xenon flasher unit was mounted on each telescope and the flashers located by finder scopes mounted on the source and receiving telescopes. The visibility was in excess of 13km and the Xenon flashers were easily identified and telescope alignment achieved. The 18" infrared source was only used in this trial and while signal-to-noise in excess of 10 to 1 was achieved at 3.8 and 10.6 micrometers, the visible wavelengths had marginal signal-to-noise ratios. At this time, the decision was made to utilize the 10" source to increase the signal output in the visible and near infrared bands.

A second feasibility trial was then conducted to verify the increase in signal-to-noise at these wavelengths using the 10" source (greybody #2). The results of this trial showed a satisfactory S/N ratio in the visible and near infrared wavelengths and the two-source system was judged

ready for calibration. However, during the second trial, it was noted that when the sun shown nearly directly into the source telescopes, it would provide a high enough DC signal to saturate the monitor diodes. It was therefore decided to backbias the diodes with a 22½ volt battery and operate the monitors in a photoconductive mode. Additionally, a baffled, blackened tube was fitted to end of the monitor diodes to reduce the amount of stray light reaching the detector. During both trials, the germanium detector was not avilable for use and therefore the actual verification of its capability to detect signals at 13.3 km has not been done. However, based upon calibration data extrapolated to 13.3 km, sufficient signal should be available for successful detection.

D. CALIBRATION TRIALS

The 2½ ton truck was then moved to the lighthouse property at Point Pinos and set up for calibration. The calibration path that was used is shown in Figure 15. Initial calibration attempts of the germanium and indium-antimonide detectors resulted in distorted signal wave forms. Analysis of the problem revealed that the detectors, although operating in the photovoltaic mode, were being biased by the background radiation received by the cells. In order to have the detectors operate in a linear portion of their voltage current curves, a small variable DC voltage

Figure 15. Calibration Path from 2½ Ton Truck to Receiving Telescope Positioned in Opening of Fog Horn Building

bias circuit was added to each detector. Under calibration conditions the indium-antimonide required .15 volts back bias while the germanium required .1 volts back bias.

In the case of the silicon, germanium and indium-antimonide detectors, the calibration value was obtained using a small dropping resistor to insure that the cell would not be operating in a non-linear portion of its voltage/current operating curve. However, a much larger dropping resistor was required to produce a useable signal output at the test distance due to the greatly reduced signal being detected. These larger dropping resistors were calibrated by lowering the source output radiation to a point where the received signal did not saturate using either resistor. After viewing the wave form on an oscilloscope to insure that the detector was operating in a linear region, the amplitude of the signal from each dropping resistor was recorded and the proportional ratio between them established.

After all the detectors and dropping resistor combinations were investigated, calibration data runs were performed for each detector. Figure 16 shows a sample of the computer output generated for each run. See Appendix A for a complete description of the data reduction method.

Calibration data were taken during a two day period in which the visibility at the calibration site was 13km one day and 7km the next day. These reduced visibility conditions have the greatest effect on the shorter visible

Dec. 14 1978
Clear
West Wind
HgCdTe
Calibration Run
18" glower

Time	= 1529
Temperature	= 11.10°C
Analog to Digital Converter resolution	= 12 bits
Relative Humidity	= 69.30
Wind Speed	= 2 knots
Range	= 360.58 meters
Wave length	= 10.6 micrometers
Gain	= 100
Detector voltage bias	= .7
Resistance	= 0
Detector temperature	= 25°C
Source voltage	= 3.55 volts
Source current	= 14.2 Amps
Source gain	= 500
Monitor temperature	= 25°C
Average detected signal voltage	= 246.11 volts
Sigma	= 0.02

Figure 16. Sample of Computer Output for a Calibration Ran.

wavelength radiation. At 0.55 micrometers the visibility conditions can be translated into a scattering coefficient by the formula [Ref. 2].

$$\mu = \frac{3.912}{Rm}$$

where

Rm = the visual range

μ = scattering coefficient at .55 micrometers

Using this expression, the visual ranges recorded during the calibration trials translate into approximately a 15% reduction of the received signal due solely to scattering and absorption. In order to include this, the calibration extinction coefficient for each wavelength will be corrected by data taken at 13.3 km under the same conditions of visual range as pertained during calibration.

IV. CONCLUSION

The system described in this report is capable of measuring atmospheric extinction in the wavelength regions of .4880, .6328, 1.06, 2.25, 3.8 and 10.66 micrometers. The system is extremely flexible and through the use of its quick change filter system, can be used to measure extinction at any of the atmospheric windows between .3 and 15 micrometers.

APPENDIX A

Description of Data Reduction Method

The computer program used in this experiment computed the mean value of the radiance in excess of noise at the calibration distance and test distance, and from this computed the extinction coefficient. Individual computations were made for all the wavelengths being detected. The program determined the value of the radiance (E) at the calibration distance and at the test distance in the following manner. Using the trigger pulse received from the UHF receiver for its timing, the NIC-80 sampled the received signal eight times and placed these values in separate registers. The computer then sampled the background signal eight times and stored these values in separate registers. The timing for the background sampling was provided by a signal time delayed from the original trigger signal. The number of additional cycles of signal and background sampled was made variable and was a data taking option. After N cycles the contents of the four center registers containing the signal were added and from this total the total of the four center background signal registers was subtracted. The difference was then divided by N times 4 and the result represented the mean signal flux detected in excess of background. The computer then used this information to provide a printout of the extinction coefficient, and other information

required to properly catalog the data.

The output of the eight signal registers and eight background registers was displayed on the Textronix CRT display. This allowed viewing the quantities to be averaged and provided a visual check that the computer was sampling the signal and background independently. A breakdown in the sampling timing would thus be seen on the display as an irregular increase in the sampled quantity (signal or noise). The averaging technique employed was designed to minimize the effects of noise and sintillation. Since both these processes have random distributions [1] and [7], averaging of the data of a large sample of points should cancel the contribution of these processes to the final result.

LIST OF REFERENCES

1. Naval Postgraduate School Report NPS61-78-003z Optical Resolution in the Turbulent Atmosphere of the Marine Boundary Layer, by E.C. Crittenden, Jr., A.W. Cooper, E.A. Milne, G.W. Rodeback, R.L. Armstead, S.H. Kalmback, D. Land and B. Katz, 24 February 1978.

2. McCartney, Earl J., Optics of the Atmosphere, p. 20-30, Wiley, 1976.

3. Goody, R.M., Atmospheric Radiation I, Theoretical Basis, p. 24-30, Oxford University Press, 1964.

4. Hudson, Richard D., Jr., Infrared System Engineering, p. 115, Wiley, 1969.

5. Jenkins, F.A. and White, H.E., Fundamental of Optics, 3rd Edition, p. 100-110, McGraw-Hill, 1957.

6. Driscoll, W.G. and Vaughn, W., Handbook of Optics, p. 16, McGraw-Hill, 1978.

7. Carlson, B.A., Communications Systems, 2nd Edition, p. 120-123, McGraw-Hill, 1975.

INITIAL DISTRIBUTION LIST

		No. Copies
1.	Defense Documentation Center Cameron Station Alexandria, Virginia 22314	2
2.	Library, Code 0142 Naval Postgraduate School Monterey, California 93940	2
3.	Department Chairman, Code 61 Department of Physics and Chemistry Naval Postgraduate School Monterey, California 93940	2
4.	Professor E.C. Crittenden, Jr., Code 61ct Department of Physics and Chemistry Naval Postgraduate School Monterey, California 93940	2
5.	LCDR James Ronald Macdonald, USN USS Dwight D. Eisenhower (CVAN-69) Fleet Post Office, New York, New York 09501	1